NUMERICAL ANALYSIS OF INDENTATION OF AN ELASTIC HEMISPHERICAL SHELL

Y.-F. Jia F.-Z. Xuan

Key Laboratory of Pressure System and Safety (MOE)
School of Mechanical and Power Engineering
East China University of Science and Technology
Shanghai, P.R. China

F.-Q. Yang *

Materials Program
Department of Chemical and Materials Engineering
University of Kentucky
Lexington, USA

ABSTRACT

Nanoindentation technique has been used to measure the elastic modulus of virus capsids, capsules, vesicles, and tubules. The principle of the nanoindentation technique is based on the elastic solution of an isotropic, homogeneous, semi-infinite material, which limits the use of nanoindentation in measuring the mechanical properties of materials of small scales. To address this limitation, Reissner's thin shell model, which is based on the point indentation on a thin shell, has been used in analyzing the indentation of thin shells. In this work, the indentation of elastic hemispherical shells of various thicknesses by a rigid, spherical indenter is analyzed, using the finite element method. The simulation results reveal the limitation of the Reissner's thin shell model. A semi-analytical relationship between the indentation depth and the indentation load is proposed, which consists of the contributions of the Hertz's local deformation, the Reissner's local flattening, and the Pogorelov's deflection of the shell. This relationship provides an analytical basis of using nanoindentation to determine the nominal contact modulus of spherical shells. The comparison between the numerical results and the experimental results in literature supports the proposed semi-analytical relationship and reveals the effect of viscoelastic characteristic of shell structures on the indentation deformation.

Keywords: Indentation (normal, micro and nano), Elastic properties, Biomaterials, Finite element analysis.

1. INTRODUCTION

Nanoindentation has been extensively used to characterize localized mechanical properties of materials. The calculation of the elastic modulus of a material from the instrumented nanoindentation is generally based on the Oliver-Pharr method (the O-P method) [1] with the assumption that the material is isotropic, homogeneous, and semi-infinite. It is very difficult to measure the intrinsic elastic modulus of materials of small sizes due to geometrical and architectural features, which limit the use of the O-P method.

Using AFM apparatus, nanoindentation experiments have been performed to evaluate the mechanical properties of small scale materials with shell-like structures, *e.g.* virus capsids [2,3], capsules [4-6], vesicles [7,8], and nanotubes, *e.g.* carbon nanotubes [9-13] and tubules [14-16]. Using the Hertz contact theory [17] to analyze the contact between a spherical tip and a multiwalled CNT, Palaci *et al*. [10] and Shen *et al*. [11] determined the radial elasticity of multiwalled CNTs, respectively. Zhao *et al*. [13] found that, for the indentation deformation of viral nanotubes by an AFM tip, the elastic response can be described by the Hertz contact theory for the indentation depth less than 1.5nm and numerical analysis is needed to describe the elastic response for the indentation depth of 5nm. Currently, there are no analytical relationships between indentation depth and indentation load available for analyzing the elastic indentation of nanotubes and shell structures with relatively large indentation depth.

Assuming the AFM indenter tip as approximately spherical, Laney *et al*. [18] used the Hertz contact theory [17] to determine the elastic properties of cholinergic synaptic with the structure of a spherical shell. Recognizing the limitation of the Hertz contact theory

* Corresponding author (fyang2@uky.edu)

DOI : 10.1017/jmech.2015.59
Copyright © 2015 The Society of Theoretical and Applied Mechanics, R.O.C.
https://doi.org/10.1017/jmech.2015.59 Published online by Cambridge University Press

and the O-P method in analyzing the nanoindentation of spherical shells, researchers [3-5,8,19] have tried to use Reissner's thin shell model [20], which is based on the linear theory of shallow shells, to calculate the elastic modulus of spherical shells of thin shell thicknesses from the nanoindentation tests. It is known that a shell can experience several deformation modes at different stages of an indentation. With the indentation depth increasing over the order of the shell thickness, the shell's cap inverts inwards to form the Pogorelov ridge, *i.e.* an axisymmetric circular ridge [21,22]. At this deformation stage, the indentation depth is a power-law function of the indentation load with a power index of 2. When the indentation load is larger than a critical load, the round ridge of the shell will lose symmetrical characteristics and the deformation becomes asymmetric. A polygonal shape with three vertices will form to reduce the global stretching. Further indentation will continue to introduce additional vertices and ridges [21,23,24].

Most modeling analyses have focused on the deformation of thin shells under a point load; nevertheless, some shells with certain thicknesses cannot be simply approximated as thin shells. Also, there always exists a finite contact area between an indenter and a solid surface, and the indenter size plays an important role in the indentation deformation of a shell structure. All of these raise an issue whether the thin shell model [20,22] is a good approximation for describing the elastic indentation of elastic, spherical shells of various thicknesses.

In this work, the indentation of an elastic hemispherical shell by a rigid, spherical indenter is analyzed, using the finite element method. The study is focused on the indentation deformation prior to the occurrence of the instability of the shell. The dependence of indentation depth on indentation load for different shell thicknesses is examined. A semi-analytical relation between the indentation load and the indentation depth is proposed. The effect of the indenter size is also discussed.

2. ANALYSIS OF THE INDENTATION DEFORMATION OF AN ELASTIC SHELL

2.1 Theoretical Models of the Indentation of an Elastic, Spherical Shell

For the elastic indentation of a spherical shell of radius ($R + t$) by a rigid spherical indenter of radius r_0, the Hertz contact theory [17] gives the relationship between the indentation depth, h, and the indentation load, P, for the contact size and the indentation depth being much less than the shell thickness as

$$h = \left(\frac{3(1-\nu^2)}{4E\sqrt{R_e}} \right)^{2/3} P^{2/3} \tag{1}$$

with E and ν being the Young's modulus and Poisson's ratio of the elastic shell, respectively. Here, $R_e = r_0(R+t)/(r_0+R+t)$, where R and t are the inner radius and the thickness of the shell, respectively. Equation (1) is reduced to the Hertz contact theory of an elastic sphere for $R = 0$. Note that several assumptions are used in the Hertz contact theory: (1) the surfaces are continuous and non-conforming, and the contact radius is much smaller than the radius of curvature of the solid surface and the characteristic demsionsions of the materials, (2) the strains within the contact zone are small, (3) both materials are elastic, homogeneous, and isotropic, and (4) the contact is frictionless.

The Reissner's thin shell model [20] represents the small indentation on a thin, spherical shell, which gives the relationship between the indentation depth, h, and indentation load, P, as

$$h = \frac{R\sqrt{3(1-\nu^2)}}{4Et^2} P \equiv \frac{1}{k_1} P \tag{2}$$

There are several assumptions used in the Reissner's thin shell model, including (1) the load applied to the spherical shell is a point load, (2) the ratio of the shell thickness to the shell radius is less than 1/10, and (3) the indentation displacement is on the order of the shell thickness. The linear load-displacement characteristic corresponds to the local flattening of the shell near the contact point [7].

For an elastic thin shell of a spherical cap with a clamped edge under the action of a point load at the apex, Pogorelov [22] used the variational method to obtain the relation of the apex deflection and the load for a relatively large indentation as

$$h = \frac{R^2}{18\pi^2 c^2 E^2 t^5} P^2 \tag{3}$$

with $c \approx 0.19$. He demonstrated that Eq. (3) can be used to describe the indentation of an elastic shell by a rigid, spherical indenter. Equation (3) gives a nonlinear load-displacement relationship instead of the linear relationship from the Reissner's thin shell model [20]. Note that the same geometrical assumptions are used in the Pogorelov's model with large deflection of the shell.

2.2 Finite Element Simulation

To mimic the AFM indentation of spherical shell-structures, such as virus capsids, capsules and vesicles, a rigid, spherical indenter of radius r_0 is pushed onto an elastic hemispherical shell at the apex, as shown schematically in Fig. 1. The inner radius and the thickness of the hemispherical shell are R and t, respectively, and the edge of the hemispherical shell is clamped at a rigid substrate. The contact between the indenter and the hemispherical shell is frictionless.

To analyze the indentation deformation of the hemispherical shell, the nonlinear finite element code of ABAQUS is used. Due to the symmetrical feature of the indentation problem, an axisymmetric model is established. The finite element model consists of 64004-node bilinear-axisymmetric-quadrilateral elements. The mesh refinement is used around the

https://doi.org/10.1017/jmech.2015.59 Published online by Cambridge University Press

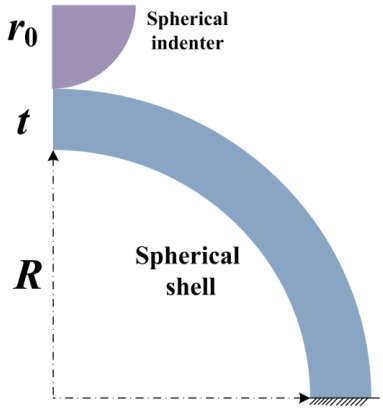


Fig. 1 Schematic of a spherical indenter acting on a hemispherical shell.

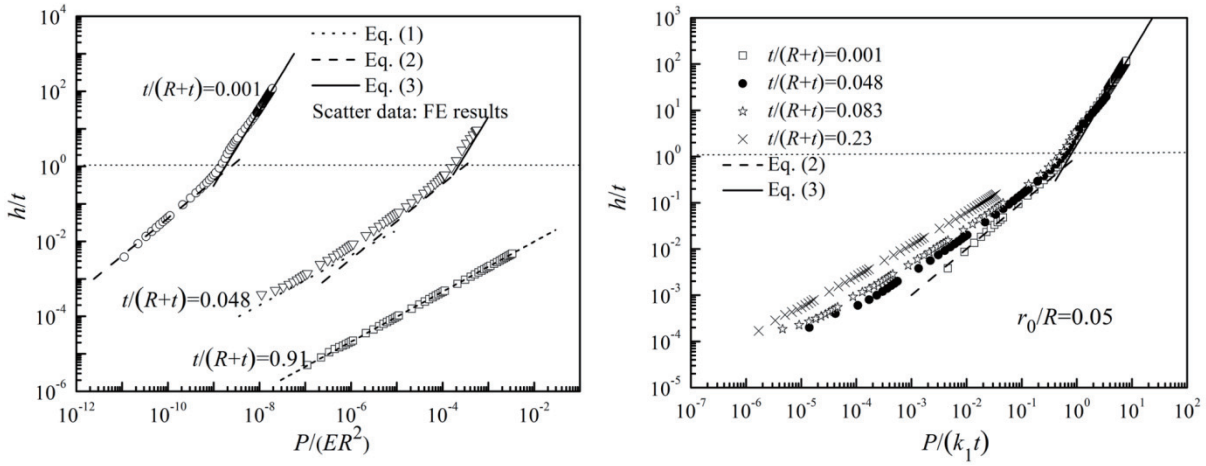
contact area. The indenter is pushed onto the surface of the hemispherical shell, using the load-controlled method. The surface-to-surface contact is used in the "Interaction setting" of ABAQUS to monitor the contact between the indenter and the surface of the elastic shell, and the frictionless tangential behavior is selected in the "Interaction Property" of ABAQUS. In the analysis, the inner radius of the hemispherical shell remains constant, while both the parameters of r_0 and t vary. The elastic modulus and Poisson's ratio of the shell are 90GPa and 0.3, respectively. The inner radius of the shell is 100μm.

3. RESULTS AND DISCUSSION

3.1 Effect of the Shell Thickness

Figure 2(a) shows the dimensionless load-displacement curves (*i.e.* h/t v.s. $P/(ER^2)$) in the log-log scales, which are obtained from the finite element simulation for the dimensionless shell thicknesses ($t/(R+t)$) of 0.001, 0.048 and 0.91 with $r_0/R = 0.05$. For comparison, the results calculated from Eqs. (1), (2) and (3) are also included in Fig. 2(a). Obviously, the load-displacement relationship cannot simply be described by any one of Eqs. (1), (2) and (3). For the shell with a shell thickness of 0.1μm (*i.e.* $t/(R+t) = 0.001$), the numerical results are in good accord with the results from Eq. (2) for $h/t < 1$ and the results from Eq. (3) for $h/t > 1$. It needs to point out that the fitted parameter of c in Eq. (3) is 0.135 instead of 0.19, as given by Pogorelov [20]. Such a difference could be attributed to that Eq. (3) was derived asymptotically in the limit of $h/t \to \infty$ while the numerical simulations cannot approach the limit. For the shell thickness of 5μm (*i.e.* $t/(R+t) = 0.048$), the numerical results agree well with the analytical results from Eq. (3) for $h/t > 1$ and the results from Eq. (1) for $h/t < 10^{-2}$. However, for $10^{-2} < h/t < 1$, the numerical results cannot be simply described by Eq. (2). These results suggest that, for a relatively thicker shell, not only the Reissner's deformation plays a role in the small indentation, but also the Hertz's contact contributes to local deformation in the regime of smaller indentation. However, for large indentation, the shell deflection follows the prediction of the Pogorelov's model. For the thick shell of the thickness of 1000μm (*i.e.* $t/(R+t) = 0.91$), the numerical results are in good agreement with the Hertz contact model, suggesting that the local deformation underneath the indenter controls the indentation behavior.

Figure 2(b) shows the other dimensionless load-displacement curves, *i.e.* h/t v.s. $P/(k_1 t)$, in the log-log scales under the same loading conditions. The parameter $k_1 = 4Et^2 / R\sqrt{3(1-\nu^2)}$ is the reciprocal of the coefficient of Eq. (2). Note that the numerical results replotted in this dimensionless form, as shown in Fig. 2(b), allows direct comparison between the Reissner's and Pogorelov's models. The results shown in Fig. 2(b) reveal the conditions at which the deviation of the numerical results from the results of the classic shell



(a) $P/(ER^2)$ (b) $P/(k_1 t)$ ($r_0/R = 0.05$)

Fig. 2 Indentation displacement, h/t, verse indentation load.

https://doi.org/10.1017/jmech.2015.59 Published online by Cambridge University Press

models occurs for the indentation of elastic shells of various shell thicknesses. For the relatively large indentation deformation, *i.e.* $h/t > 1$, all finite element results of different shell thicknesses mainly follow the results of the Pogorelov's model. The relationship between h/t and $P/(k_1 t)$ does not change significantly with the shell thickness when the shell deflection occurs. Thus, the condition of $h/t > 1$ can be regarded as a criteria for the use of the Pogorelov's model. The deviation from the Reissner's shallow shell theory occurs for $h/t < 1$ among the numerical results of different shell thicknesses. For $h/t < 1$, a higher normalized indentation load, *i.e.* $P/(k_1 t)$, is needed for a thinner shell (*i.e.* smaller value of $t/(R + t)$) with the same normalized indentation depth of h/t. Thus, for the shallow indentation on shells of certain thicknesses, the indentation load-displacement relationship follows the Hertz contact model instead of the Reissner's shallow shell model for very small indentation.

Generally, the Hertzian contact theory describes the contribution of local deformation to the overall deformation response of a hemispherical shell, and the "thin-shell models" describe the contribution of the shell ("global") deformation. The indentation deformation of an elastic hemispherical shell consists of the contribution of local deformation and the shell deformation. If the interaction between the local deformation and the shell deformation is negligible, one can use the superposition principle to obtain the resultant indentation depth as

$$\begin{aligned} h &= h_H + h_R + h_P \\ &= \alpha\left(\frac{3(1-\nu^2)}{4E\sqrt{R_e}}\right)^{2/3} P^{2/3} + \beta\frac{(R+t/2)\sqrt{3(1-\nu^2)}}{4Et^2}P \\ &\quad + \gamma\frac{(R+t/2)^2}{18\pi^2 c^2 E^2 t^5}P^2 \end{aligned} \tag{4}$$

where α, β and γ are the weighting factors, which describe the contribution of the three deformation modes, respectively, to the total indentation displacement and depend on the shell thickness, the radius of indenter, and the material properties of the shell. The first term on the right side represents the contribution of the local deformation underneath indenter, being referred to as the Hertz local deformation, and the second term represents the contribution of the local flattening of the shell, *i.e.* the Reissner's local flattening, and the third term represents the contribution of the deflection of the shell, being referred to as the Pogorelov's shell deflection. Usually, the inner radius of the shell, R, is approximately regarded as the radius of the shell in the thin shell theory. Here, the radius of the position of the centerline of the shell, *i.e.* $R + t/2$, is used in the analysis due to the consideration of various shell thicknesses. From Eq. (4), one obtains the contact stiffness, S, as

$$\begin{aligned} S \equiv \frac{dP}{dh} = \Bigg[&\frac{2\alpha}{3}\left(\frac{3(1-\nu^2)}{4E\sqrt{R_e}}\right)^{2/3} P^{-1/3} + \beta\frac{(R+t/2)\sqrt{3(1-\nu^2)}}{4Et^2} \\ &+ \gamma\frac{(R+t/2)^2}{9\pi^2 c^2 E^2 t^5}P \Bigg]^{-1} \end{aligned} \tag{5}$$

Note that one can calculate the elastic modulus of the elastic shell from the contact stiffness if all the weighting factors, contact stiffness and Poisson ratio are known.

Figure 3 shows the fitting curves of the numerical results for four shell thicknesses, using Eq. (4). The fitting process was performed using the nonlinear curve fit of the Origin software, which is based on the least square method. In the fitting, the fitting parameters were set to be larger than 0. The indentation load required for producing the same indentation depth increases with the increase of the shell thickness, as expected. Note that similar behavior is also observed for the elastic indentations by rigid, spherical indenters of 1 and 30μm in radius, respectively, which are not included here. Equation (4) fits well with the indentation load-displacement curves for a wide range of the shell thicknesses. For the case of t = 5μm ($t/(R + t)$ = 0.048), the fitting curve can describe the numerical results from the extremely small indentation displacement to the large indentation displacement.

Furthermore, the contributions of the corresponding deformation modes of the shell to the overall indentation displacement at different indentation displacements could be quantitatively examined from Eq. (4), in which the parameters of h_H, h_R and h_P are defined in Eqs. (1), (2) and (3), respectively. Thus, the parameters of h_H/h, h_R/h and h_P/h determine the contributions of the Hertzian local deformation, the Reissner's local flattening and the Pogorelov's shell deflection, respectively. Figure 4 shows the contributions of the three deformation modes to the overall indentation displacement for four shell thicknesses. For the thinnest shell of

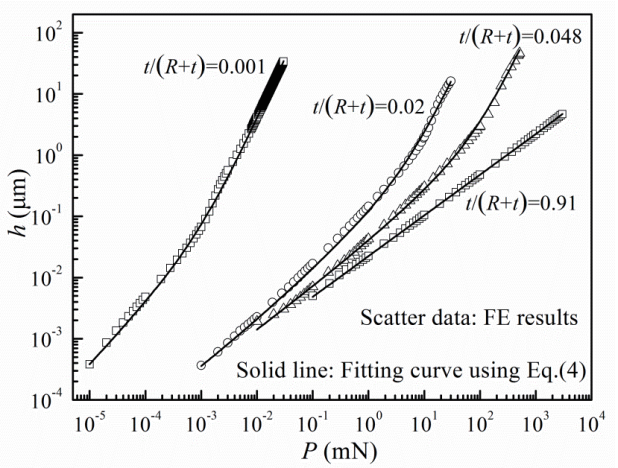


Fig. 3 Fitting curves of the numerical results for four shell thicknesses, using Eq. (4).

https://doi.org/10.1017/jmech.2015.59 Published online by Cambridge University Press

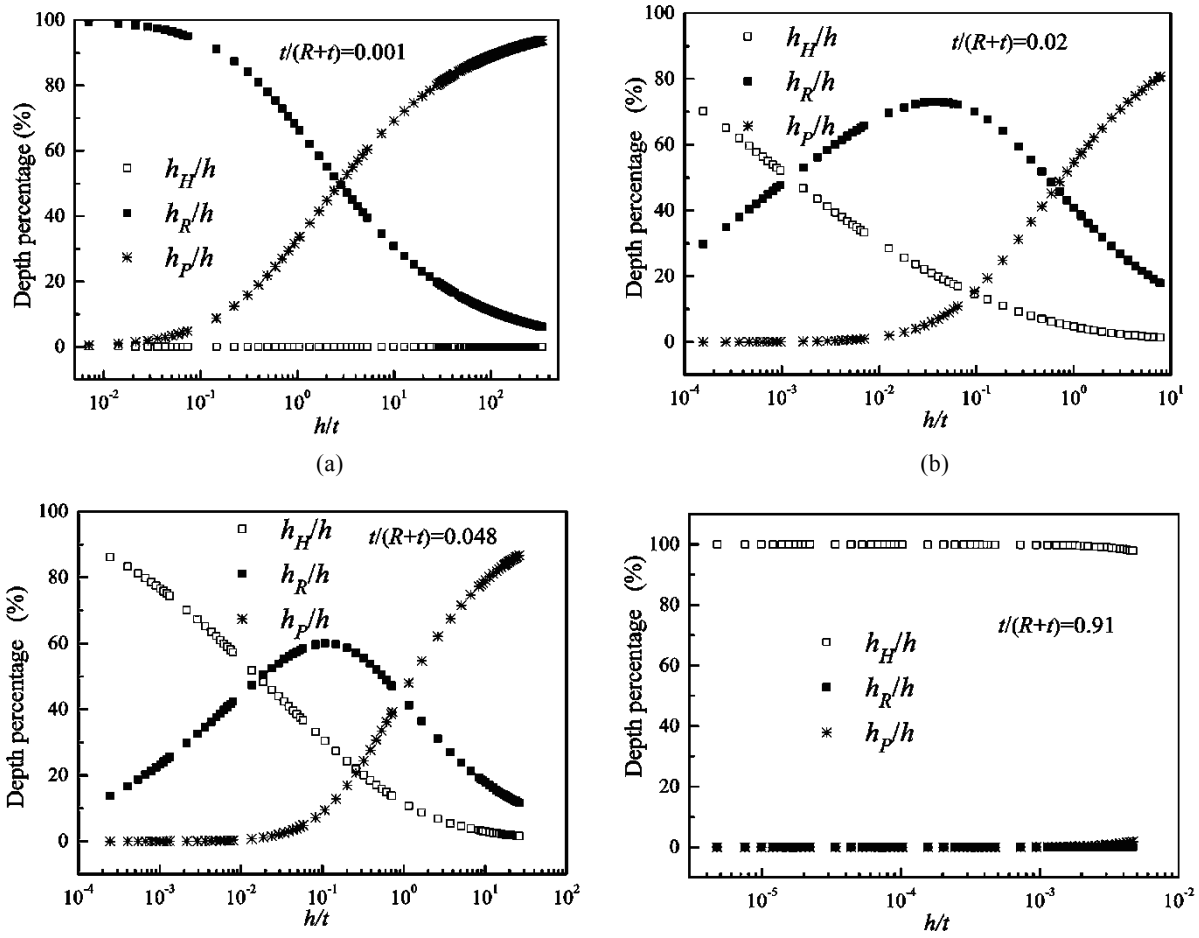


Fig. 4 Proportion of the Hertz's local deformation (h_H / h), the Reissner's local flattening (h_R / h) and the Pogorelov's global deflection (h_P / h) in Eq. (4) as a function of the indentation depth, h/t, for four shell thicknesses.

$t/(R + t) = 0.001$ (as shown in Fig. 4(a)), the maximum of the three values for small indentation is h_R/h while the other two values are close to 0. This result indicates that the Reissner's local flattening is dominant. With the increase of the indentation depth, the contribution of the Reissner's local flattening decreases, and the contribution of the Pogorelov's deflection of shell increases and becomes larger than the local flattening. For the large indentation, the shell's deflection is dominant. Moreover, one can note that the contribution of the Hertzian local deformation remains near zero for the range of the indentation depth. For the relatively thicker shell, *e.g.* $t/(R + t) = 0.02$ and 0.048 (as shown in Figs. 4(b) and 4(c)), the contribution of the Hertzian local deformation, *i.e.* the value of h_H/h, for small indentation becomes more dominant with increasing the shell thickness, while the contribution of the Reissner's local flattening decreases. With the increase of the indentation displacement, the contribution of the Hertzian local deformation decreases gradually, and the contribution of the Pogorelov's shell deflection increases for $h/t > 10^{-2}$. For the thickest shell of $t/(R + t) = 0.91$ (as shown in Fig. 4(d)), the main contribution in the whole range of the indentation displacement is the Hertzian local deformation, and the other two contributions basically are near zero due to the insignificant shell deformation for the thickest shell.

In general, it is extremely difficult to develop an analytical function for describing the indentation deformation of an elastic shell. However, some criteria can still be used, regarding the conditions under which the three models can be used individually. The Hertz contact model is appropriate for the shallow indentation on thick shells. The Reissner's model can be used for thin shells with the indentation displacement being on the order of the shell thickness. The Pogorelov's model can be used for both thin shells and thick shells in analyzing the shell deflection with $h/t > 1$, as shown in the Fig. 2(b).

As described above, the parameter of h_H/h is associated with the Hertzian local deformation. To examine the contribution of this local deformation, the shell thickness under the lowest contact point between the indenter and the shell during the indentation was obtained from the finite element analysis, *i.e.* t_R, which is shown in Fig. 5(a). The parameter of $(t - t_R)/h$ is the dimensionless penetration into the shell, which represents the local deformation underneath the indenter. Figure 5b shows the comparison of the Hertzian local deformation calculated by Eq. (4), *i.e.* h_H/h, with the

https://doi.org/10.1017/jmech.2015.59 Published online by Cambridge University Press

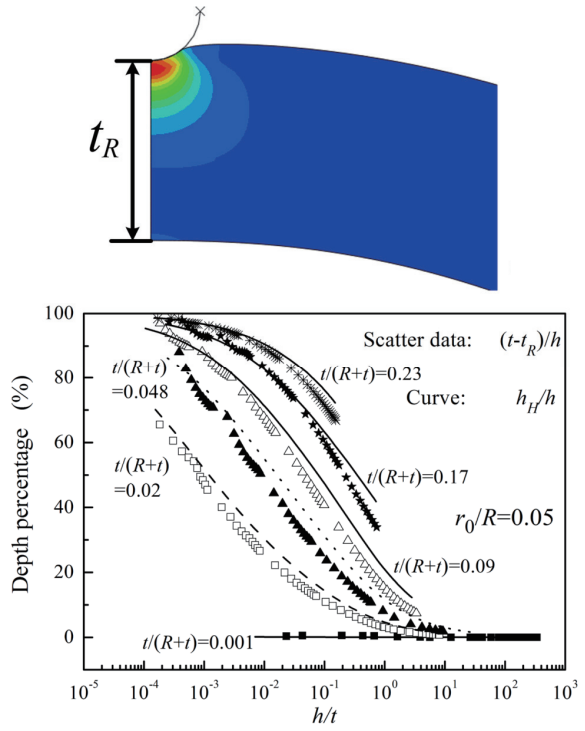


Fig. 5 (a) Shell thickness, t_R, under the lowest contact point between the indenter and the shell during indentation, and (b) comparison of h_H/h with $(t - t_R)/h$ for various shell thicknesses (r_0/R = 0.05).

penetration into the shell, *i.e.* $(t - t_R)/h$, for different shell thicknesses. The curves of h_H/h as a function of the indentation displacement, h/t, agree well with the results of $(t - t_R)/h$ for the shell thicknesses, which indicates the parameter of h_H/h can be used to describe the Hertzian local deformation. Also, it is evdient that the role of the Hertzian local deformation is more significant for thicker shells.

3.2 Effect of Indenter Radius

The effect of the indenter radius (r_0) on the indentation load-displacement curves was also investigated in this study. Figure 6 show the indentation load-displacement curves, h/t verse $P/(ER^2)$, for four shell thicknesses, representing a thin shell to a thick shell. Three dimensionless radii of 0.01, 0.05 and 0.3 were used. The force required to produce the same indentation displacement increases with the increase of the indenter radius for the shell of the same thickness. For the indentation displacement with $h/t > 1$, *i.e.* the large indentation deformation, the indenter radius doesn't have a significant effect on the indentation load-displacement curve, which indicates the deflection of the shell is independent on the indenter radius used in the analysis. For the indentation displacement with $h/t < 1$, *i.e.* the small deformation, the effect of the indenter radius on the indentation load-displacement curve becomes complicated. For the thinnest shell of

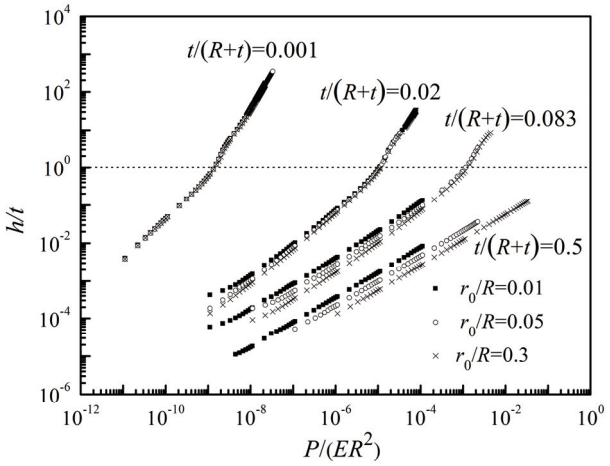


Fig. 6. Variation of indentation displacement, h/t, with indentation load, $P/(ER^2)$, for various shell thicknesses and three indenter radii.

t = 0.1μm, it is very difficult to distinguish the differences in the indentation curves for the three indenter radii. However, with increasing the shell thickness, the indentation load-displacement curves increasingly depend on the indenter radius. The indentation by an indenter of a larger indenter radius will have a more significant effect on the indentation load-displacement curves for small indentation displacement. The effect of the indenter radius on the indentation load-displacement curves is due to the Hertzian local deformation, associated with the effective radius for the contact deformation, as given in Eq. (1).

3.3 Comparison Between Numerical Results and Experimental Results

There are several works, which have provided the load-displacement data for the indentation of shell structures. Figure 7 shows the comparison between the numerical results and the experimental results reported in literature. Also, the finite element results of the indentation onto a thin shell given by Vella *et al*. [25] are included in Fig. 7. Obviously, the simulation results obtained in our study are in good accord with the results Vella *et al*. [25].

The indentation deformation of the synthetic hollow silica sphere was characterized by an AFM [19], which shows the linear increase of the indentation displacement with the indentation load. Note that the experimental study by Zhang *et al*. [19] falls into the small deformation regime of the numerical simulation of the indentation of the thin shell (t = 0.1). The experimental results of the large indentation deformation of thin spherical shells given by Nasto *et al*. [21] are replotted in Fig. 7, which are basically in accord with the numerical results of thin shells in both the small and large deformation regimes. Delorme *et al*. [7] used the Reissner's model to estimate the elastic property of the catanionic hollow faceted polyhedrons from the indentation displacement-load curves in the small deformation regime. Their displacement-load data in both the small and large deformation regimes are

https://doi.org/10.1017/jmech.2015.59 Published online by Cambridge University Press

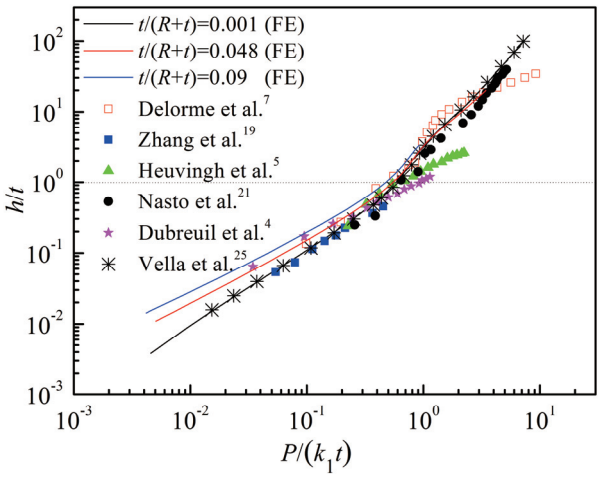


Fig. 7 Comparison of the numerical results of the indentation of shells of various shell thicknesses with the experimental results in literature.

compared with the numerical results in Fig. 7, which shows good agreement with the numerical results in the small deformation regime. In the large deformation regime, the experimental results deviate from the numerical results, which may be attributed to the influence of the polyhedron shape of the shell on large indentation. The experimental data of the polyelectrolyte capsules of Fery and co-workers [4,5] are also plotted in Fig. 7. In the small deformation regime, the indentation displacement-load curves deviate from the results of the thin-shell model, but coincide with the numerical results of the shell of a larger thickness. Thus, simply using the Reissner's model in measuring the elastic modulus of an elastic shell could introduce some measurement errors. Also, the power index of the experimental results of $h/t \sim P/(k_1 t)$ doesn't show significant changes with increasing the indentation load, which is in contrast to the elastic analysis of the shell deformation during indentation. Such a discrepancy could be in part due to that the indentation testing was performed in a liquid environment. In addition, the viscoelastic characteristic of the polyelectrolyte capsules could also affect the shell deformation.

To examine the effect of viscoelastic deformation on the indentation behavior, a simple viscoelastic model is used to model the viscoelastic behavior of the shell and to reveal the possible effect of viscoelasticity on the indentation load-displacement curves. Figure 8(a) shows the standard linear solid model used in the finite element analysis. Using a single-term Prony series for the shear relaxation modulus, the viscoelastic characteristics of the standard linear solid model can be approximated as

$$g(t) = 1 - g_1(1 - e^{-t/\tau_1}) \tag{6}$$

where g_1 is the shear relaxation modulus ratio, and τ_1 is the shear relaxation time. It is assumed that no volumetric relaxation occurs during the deformation, so that the bulk relaxation modulus ratio is zero. The values of g_1 and τ_1 of the viscoelastic model used in the simulation are 0.2 and 100s, respectively. The loading time was 10s. Figure 8(b) shows the comparison of the indentation load-displacement curves between the elastic and the viscoelastic thin shells. The indentation displacement displays an approximately linear dependence on the indentation load even under the large load for the indentation of the viscoelastic shell in contrast to the power law relationship with a power index of 2 for the indentation of an elastic thin shell. The numerical results from the simulation of the indentation of a viscoelastic shell shows that the variation of the indentation displacement with the indentation load is similar to the experimental results of the indentation of polyelectrolyte capsules [4,5]. Such a result reveals the mechanism controlling the deviation of the indentation displacement-load data for the indentation of polyelectrolyte capsules from the indentation curve for the indentation of an elastic thin shell at large indentation depth. Note that the indenter for the indentation of the elastic shell experiences a larger displacement than that of the viscoelastic shell for a larger indentation load. Such trend is likely due to the different deformation modes of the shells, as shown in the inserted figures for the deformation profile of the elastic and viscoelastic shells at the same indentation depth of $h/t = 25$. The indentation of a viscoelastic shell introduces more local deformation than that of an elastic shell. A larger deflection of the elastic shell occurs than that of the viscoelastic shell for the same larger indentation load.

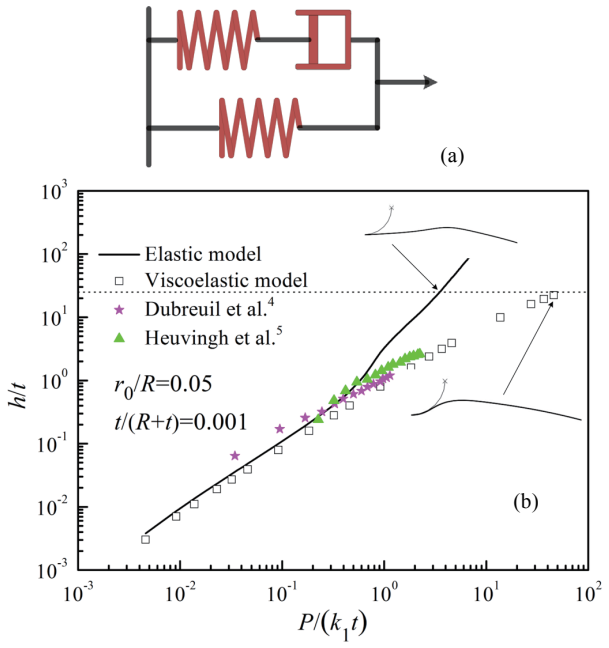


Fig. 8 (a) Standard linear solid model used for the finite element analysis of the indentation of a viscoelastic shell, (b) comparison of the indentation load-displacement curve of an elastic shell with that of a viscoelastic shell ($r_0/R = 0.05$ and $t/(R + t) = 0.001$). The inserts show the deformation of the elastic shell and the viscoelastic shell at the same indentation depth, respectively.

https://doi.org/10.1017/jmech.2015.59 Published online by Cambridge University Press

It is worth mentioning that plastic deformation generally occurs during the indentation of a thin shell in most experimental conditions, which can cause the difference between experimental results and the numerical results for elastic indentation. The effect of the plastic deformation of thin shells on the indentation curves will be examined and compared with the effect of viscous flow in the future.

4. CONCLUSIONS

The spherical indentation of hemispherical shells was studied, using the finite element simulation. The effect of the shell thickness and the indenter radius on the indentation load-displacement curves was analyzed. The results are summarized below:

1. A semi-analytical relationship between the indentation depth and the indentation load for various shell thicknesses was proposed, which consists of the contributions of the Hertzian local deformation, the Reissner's local flattening, and the Pogorelov's deflection of the shell.
2. For a thick shell, the Hertzian local deformation is dominant at the shallow indentation regime. With the indentation depth increasing to a certain value, the contribution of the Reissner's local flattening becomes significant. When the indentation depth is larger than the shell thickness, the Pogorelov's shell deflection become dominant.
3. For the indenter radius used in the analysis, the indentation load-displacement curves are approximately independent on the indenter radius for very thin shells and dependent on the indenter radius for thick shells at shallow indentation.
4. Comparing numerical results with the experimental results in literature, it is found that the use of the Reissner's model in calculating the elastic modulus of relatively thicker shells can introduce the measurement error.
5. The viscoelastic characteristic of a shell influences the indentation response at large indentation.

ACKNOWLEDGEMENTS

FZX is grateful for the support provided by the National Natural Science Foundation of China (51325504). YFJ is grateful for the support provided by the Fundamental Research Funds for the Central Universities (22A201514024).

REFERENCES

1. Oliver, W. C. and Pharr, G. M., "An Improved Technique for Determining Hardness and Elastic-Modulus Using Load and Displacement Sensing Indentation Experiments," *Journal of Materials Research*, **7**, pp. 1564–1583 (1992).
2. Carrasco, C., Carreira, A., Schaap, I. A. T., Serena, P. A., Gomez-Herrero, J., Mateu, M. G. and Pablo, P. J., "DNA-Mediated Anisotropic Mechanical Reinforcement of a Virus," *Proceedings of the National Academy of Sciences of the United States of America*, **103**, pp. 13706–13711 (2006).
3. Ivanovska, I. L., de Pablo, P. J., Ibarra, B., Sgalari, G., MacKintosh, F. C., Carrascosa, J. L., Schmidt, C. F. and Wuite, G. J. L., "Bacteriophage Capsids: Tough Nanoshells with Complex Elastic Properties," *Proceedings of the National Academy of Sciences of the United States of America*, **101**, pp. 7600–7605 (2004).
4. Dubreuil, F., Elsner, N. and Fery, A., "Elastic Properties of Polyelectrolyte Capsules Studied by Atomic Force Microscopy and RICM," *European Physical Journal E*, **12**, pp. 215–221 (2003).
5. Heuvingh, J., Zappa, M. and Fery, A., "Salt Softening of Polyelectrolyte Multilayer Capsules," *Langmuir*, **21**, pp. 3165–3171 (2005).
6. Zhang, L. J., D'Acunzi, M., Kappl, M., Imhof, A., van Blaaderen, A., Butt, H. J., Graf, R. and Vollmer, D., "Tuning the Mechanical Properties of Silica Microcapsules," *Physical Chemistry Chemical Physics*, **12**, pp. 15392–15398 (2010).
7. Delorme, N. and Fery, A., "Direct Method to Study Membrane Rigidity of Small Vesicles Based on Atomic Force Microscope Force Spectroscopy," *Physical Review E*, **74**, p. 030901 (2006).
8. Delorme, N., Dubois, M., Garnier, S., Laschewsky, A., Weinkamer, R., Zemb, T. and Fery, A., "Surface Immobilization and Mechanical Properties of Catanionic Hollow Faceted Polyhedrons," *Journal of Physical Chemistry B*, **110**, pp. 1752–1758 (2006).
9. Minary-Jolandan, M. and Yu, M. F., "Reversible Radial Deformation up to the Complete Flattening of Carbon Nanotubes in Nanoindentation," *Journal of Applied Physics*, **103**, p. 073516 (2008).
10. Palaci, I., Fedrigo, S., Brune, H., Klinke, C., Chen, M. and Riedo, E., "Radial Elasticity of Multiwalled Carbon Nanotubes," *Physical Review Letters*, **94**, p. 175502 (2005).
11. Shen, W. D., Jiang, B., Han, B. S. and Xie, S. S., "Investigation of the Radial Compression of Carbon Nanotubes with a Scanning Probe Microscope," *Physical Review Letters*, **84**, pp. 3634–3637 (2000).
12. Yu, M. F., Kowalewski, T. and Ruoff, R. S., "Investigation of the Radial Deformability of Individual Carbon Nanotubes under Controlled Indentation Force," *Physical Review Letters*, **85**, pp. 1456–1459 (2000).
13. Zhao, Y., Ge, Z. B. and Fang, J. Y., "Elastic Modulus of Viral Nanotubes," *Physical Review E*, **78**, p. 031914 (2008).
14. Kis, A. *et al.,* "Nanomechanics of Microtubules," *Physical Review Letters*, **89**, p. 248101 (2002).
15. Zhao, Y., An, L. A. and Fang, J. Y., "Buckling Instability of Lipid Tubules with Multibilayer Walls under Local Radial Indentation," *Physical Review E*,

https://doi.org/10.1017/jmech.2015.59 Published online by Cambridge University Press

80, p. 021911 (2009).
16. Zhao, Y., Tamhane, K., Zhang, X. J., An, L. N. and Fang, J. Y., "Radial Elasticity of Self-Assembled Lipid Tubules," *ACS Nano*, **2**, pp. 1466–1472 (2008).
17. Hertz, H., "Über die Berührung Fester Elastischer Körper," *Journal für die Reine und Angewandte Mathematik*, **92**, pp. 156–171 (1882).
18. Laney, D. E., Garcia, R. A., Parsons, S. M. and Hans-ma, H. G., "Changes in the Elastic Properties of Cholinergic Synaptic Vesicles as Measured by Atomic Force Microscopy," *Biophysical Journal*, **72**, pp. 806–813 (1997).
19. Zhang, L., D'Acunzi, M., Kappl, M., Auernhammer, G. K., Vollmer, D., van Kats, C. M. and van Blaaderen, A., "Hollow Silica Spheres: Synthesis and Mechanical Properties," *Langmuir*, **25**, pp. 2711–2717 (2009).
20. Reissner, E., "Stresses and Small Displacements of Shallow Spherical Shells.2," *Journal of Mathematics and Physics*, **25**, pp. 279–300 (1946).
21. Nasto, A., Ajdari, A., Lazarus, A., Vaziri, A. and Reis, P. M., "Localization of Deformation in Thin Shells under Indentation," *Soft Matter*, **9**, pp. 6796–6803 (2013).
22. Pogorelov, A. V., *Bendings of Surfaces and Stability of Shells*, AMS Bookstore, Providence, RI, (1988).
23. Vaziri, A., "Mechanics of Highly Deformed Elastic Shells," *Thin-Walled Structures*, **47**, pp. 692–700 (2009).
24. Vaziri, A. and Mahadevan, L., "Localized and Extended Deformations of Elastic Shells," *Proceedings of the National Academy of Sciences of the United States of America*, **105**, pp. 7913–7918 (2008).
25. Vella, D., Ajdari, A., Vaziri, A. and Boudaoud, A., "The Indentation of Pressurized Elastic Shells: From Polymeric Capsules to Yeast Cells," *Journal of the Royal Society Interface*, **9**, pp. 448–455 (2012).

(Manuscript received February 24, 2015,
accepted for publication May 11, 2015.)

https://doi.org/10.1017/jmech.2015.59 Published online by Cambridge University Press